

An Adaptive Control Strategy for Neural Network based Optimal Quadcopter Controllers

Robin Ferede¹, Guido C.H.E. de Croon¹, Christophe De Wagter¹, Dario Izzo²

Abstract—Developing optimal controllers for aggressive high-speed quadcopter flight is a major challenge in the field of robotics. Recent work has shown that neural networks trained with supervised learning can achieve real-time optimal control in some specific scenarios. In these methods, the networks (termed G&C Nets) are trained to learn the optimal state feedback from a dataset of optimal trajectories. An important problem with these methods is the reality gap encountered in the sim-to-real transfer. In this work, we trained G&C Nets for energy-optimal end-to-end control on the Bebop drone and identified the unmodeled pitch moment as the main contributor to the reality gap. To mitigate this, we propose an adaptive control strategy that works by learning from optimal trajectories of a system affected by constant external pitch, roll and yaw moments. In real test flights, this model mismatch is estimated onboard and fed to the network to obtain the optimal rpm command. We demonstrate the effectiveness of our method by performing energy-optimal hover-to-hover flights with and without moment feedback. Finally, we compare the adaptive controller to a state-of-the-art differential-flatness-based controller in a consecutive waypoint flight and demonstrate the advantages of our method in terms of energy optimality and robustness.

Index Terms—real-time optimal control, supervised learning, G&CNet, end-to-end control, reality gap, sim-to-real transfer

I. INTRODUCTION

NOWADAYS there is an increasing demand for autonomous quadcopters for various military and civilian applications [1]. For many applications such as emergency response, inspection, delivery or racing the drone must fly as fast, and as energy efficient as possible [2]. However, developing autonomous systems for aggressive high-speed flight still poses many challenges. One of these challenges is developing computationally efficient optimal control algorithms that take into account non-linear dynamics and actuator limits.

Current state-of-the-art research on time-optimal quadcopter control focuses on making controllers track a reference guidance trajectory. Popular tracking methods include the differential-flatness-based controller (DFBC) [3]–[6] and the traditional nonlinear-model-predictive controller (NMPC) [7]–[12]. While the DFBC is more computationally efficient, traditional NMPC has gained a lot of popularity

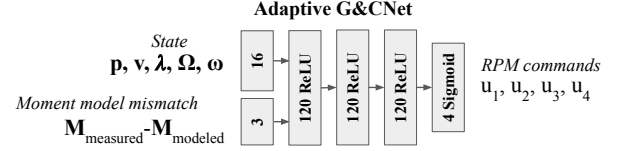


Fig. 1. Bebop drone controlled by an energy-optimal G&CNet. Although we perturb the dynamics by adding a weight on one side, the Bebop drone flies through the 3×4m track by adapting its rpm command based on the state and the moment model mismatch.

in quadcopter control due to advances in hardware. The advantages of NMPC over DFBC are improved tracking accuracy for dynamically infeasible trajectories as well as improved robustness to model mismatch [13] (especially by means of adaptive algorithms [10], [14]). Furthermore, in recent work, a traditional NMPC method was shown to outperform human pilots in a drone-racing task by tracking offline-generated time-optimal trajectories [15]. An inherent limitation with all of these methods is that the aggressiveness and efficiency of the performed maneuver are fully determined by the trajectory to be tracked. Moreover, the generation of time-optimal trajectories is often computationally intensive and requires either offline calculation, or an online sub-optimal simplification in the form of polynomial guidance [4], [6], [16], point mass trajectories [12], [17] or numerical approximation methods [18]–[20]. Furthermore, to add control authority to the NMPC method, a margin is often defined to lower the actuator limits used for the trajectory generation. This reduces optimality since time-optimal control relies on saturating the actuators in a bang-bang fashion. A recent trend in quadcopter control research is the application of machine learning techniques to trajectory generation and tracking. Deep neural networks have been trained for trajectory generation using reinforcement learning [21] and supervised machine learning [22]. Similarly, trajectory tracking has been improved by training neural networks either from flight data [23], [24] or from simulation

*This work was supported by ESA

¹The authors are with the Micro Air Vehicle Lab of the Faculty of Aerospace Engineering, Delft University of Technology, 2629 HS Delft, The Netherlands R.Ferede@tudelft.nl, G.C.H.E.deCroon@tudelft.nl, C.deWagter@tudelft.nl

²The authors are with the Advanced Concepts Team, European Space Agency, Keplerlaan 1, 2201 AZ, Noordwijk, The Netherlands. Dario.Izzo@esa.int

data [25], [26]. Another research line [27]–[29] proposes an alternative to the trajectory tracking-based control methods by combining guidance and control into a single neural network (termed G&CNet) which is trained to imitate the optimal state feedback from a dataset of time-optimal trajectories. Once trained, the G&CNet provides a computationally efficient way to compute the optimal control onboard the quadcopter without requiring any trajectory (re)planning. With a real flight test, this has been demonstrated to work for longitudinal trajectories based on a simplified, 2-dimensional quadcopter model [27]. In these experiments, the G&CNet was used to calculate thrust and pitch acceleration commands which were tracked by an INDI [30] controller.

In this article, we investigate for the first time an end-to-end, i.e., state-to-rpm G&CNet for a 3-dimensional quadcopter model taking into account drag, aerodynamic effects and actuator delays. Unlike the previous work [27] this network can fully exploit the 6-degrees-of freedom of the quadcopter model. Furthermore, our network directly calculates the rpm motor commands which allows us to take advantage of the actuator's limits without being limited by a low-level controller. The biggest obstacle with this approach is the reality gap between the model and the real world. In this research, we identify this reality gap for energy-optimal flight and propose an adaptive method to mitigate the most significant effects namely: unmodeled roll, pitch and yaw moments. Furthermore, we benchmark our controller's performance against a state-of-the-art differential-flatness-based controller using an identical setup with the same hardware. Here we demonstrate the advantages of our method in terms of energy-optimality and robustness.

II. METHODOLOGY

A. Quadcopter model

The quadcopter's state and control input are defined by

$$\mathbf{x} = [\mathbf{p}, \mathbf{v}, \boldsymbol{\lambda}, \boldsymbol{\Omega}, \boldsymbol{\omega}]^T \quad \mathbf{u} = [u_1, u_2, u_3, u_4]^T$$

Where $\mathbf{p} = [x, y, z]$ and $\mathbf{v} = [v_x, v_y, v_z]$ are the position and velocity in the world frame, $\boldsymbol{\Omega} = [p, q, r]$ is the angular velocity in body frame, $\boldsymbol{\lambda} = [\phi, \theta, \psi]$ are the Euler angles that describe the orientation of the body frame and $\boldsymbol{\omega} = [\omega_1, \omega_2, \omega_3, \omega_4]$ are the angular velocities of each of the propellers in rpm. The control input \mathbf{u} contains the normalized rpm commands $u_i \in [0, 1]$. The system dynamics are described by:

$$\begin{aligned} \dot{\mathbf{p}} &= \mathbf{v} & \dot{\mathbf{v}} &= \mathbf{g} + R(\boldsymbol{\lambda})\mathbf{F} \\ \dot{\boldsymbol{\lambda}} &= Q(\boldsymbol{\lambda})\boldsymbol{\Omega} & I\dot{\boldsymbol{\Omega}} &= -\boldsymbol{\Omega} \times I\boldsymbol{\Omega} + \mathbf{M} \\ \dot{\boldsymbol{\omega}} &= ((\omega_{max} - \omega_{min})\mathbf{u} + \omega_{min} - \boldsymbol{\omega})/\tau \end{aligned} \quad (1)$$

Where $\mathbf{g} = [0, 0, g]^T$ is the gravitational acceleration, I is the moment of inertia matrix given by $\text{diag}(I_x, I_y, I_z)$, ω_{min} and ω_{max} are the minimum and maximum propeller rpm limits and τ is the first order delay parameter of the actuator model. Furthermore, $R(\boldsymbol{\lambda})$ is the rotation matrix that describes the orientation of the body frame and $Q(\boldsymbol{\lambda})$ denotes a transformation between angular velocities and

Euler angles. $\mathbf{F} = [F_x, F_y, F_z]^T$ is the specific force acting on the quadcopter in the body frame which we model as a function of the body velocities and the propeller RPMs using a thrust and drag model based on [31]:

$$\begin{aligned} F_x &= -k_x v_x^B \sum_{i=1}^4 \omega_i & F_y &= -k_y v_y^B \sum_{i=1}^4 \omega_i \\ F_z &= -k_\omega \sum_{i=1}^4 \omega_i^2 - k_z v_z^B \sum_{i=1}^4 \omega_i - k_h (v_x^{B2} + v_y^{B2}) \end{aligned} \quad (2)$$

Similarly, $\mathbf{M} = [M_x, M_y, M_z]^T$ is the moment acting on the quadcopter which we model with the following equations:

$$\begin{aligned} M_x &= k_p (\omega_1^2 - \omega_2^2 - \omega_3^2 + \omega_4^2) + k_{pv} v_y^B \\ M_y &= k_q (\omega_1^2 + \omega_2^2 - \omega_3^2 - \omega_4^2) + k_{qv} v_x^B \\ M_z &= k_{r1} (-\omega_1 + \omega_2 - \omega_3 + \omega_4) \\ &\quad + k_{r2} (-\dot{\omega}_1 + \dot{\omega}_2 - \dot{\omega}_3 + \dot{\omega}_4) - k_{rr} r \end{aligned} \quad (3)$$

See Table I for the parameter values identified for our platform.

B. Energy optimal control problem

Given a state space X and set of admissible controls U , the goal is to find a control trajectory $\mathbf{u} : [0, T] \rightarrow U$ that steers the system from an initial state \mathbf{x}_0 to some target state $S \subset X$ in time T while minimizing some cost function. The energy optimal control problem can be formulated as

$$\begin{aligned} \underset{\mathbf{u}, T}{\text{minimize}} \quad & E(\mathbf{u}, T) = \int_0^T \|\mathbf{u}(t)\|^2 dt \\ \text{subject to} \quad & \dot{\mathbf{x}} = f(\mathbf{x}, \mathbf{u}) \quad \mathbf{x}(0) = \mathbf{x}_0 \quad \mathbf{x}(T) \in S \end{aligned} \quad (4)$$

Similar to [27] the control problem is transformed into a Nonlinear Programming (NLP) problem using Hermite Simpson transcription. The trajectories $\mathbf{x}(t), \mathbf{u}(t)$ are discretized into $N + 1$ points with a time step $\Delta t = T/N$ such that $\mathbf{x}_k = \mathbf{x}(k\Delta t)$ and $\mathbf{u}_k = \mathbf{u}(k\Delta t)$. Using the AMPL [33] modeling language with the SNOPT NLP solver [34], the optimal (discretized) trajectory $\mathbf{x}_0^* \dots \mathbf{x}_N^*$ and $\mathbf{u}_0^* \dots \mathbf{u}_N^*$ can be computed.

C. Dataset generation and network training

A dataset is created by generating optimal trajectories for a range of initial conditions. From these trajectories, a dataset of state-action pairs can be obtained of the form $(\mathbf{x}_i^*, \mathbf{u}_i^*) \quad i = 0, \dots, N$. We use these state-action pairs to train a Neural Network $f_N : X \rightarrow U$ to approximate the optimal feedback¹ that maps \mathbf{x}_i^* to \mathbf{u}_i^* . In all our experiments we use a neural network with 3 hidden layers of 120 neurons with ReLU activation and an output layer of 4 neurons with Sigmoid activation (Fig 1). Similar to [27] we use the mean squared error loss function:

$$l = \|f_N(\mathbf{x}_i^*) - \mathbf{u}_i^*\|^2$$

¹From [28]: "the Hamilton-Jacobi-Bellman equations are important here as they imply the existence and uniqueness of an optimal state-feedback $\mathbf{u}^*(\mathbf{x})$ which, in turn, allow to consider universal function approximators such as deep neural networks to represent it."

TABLE I

MODEL PARAMETERS FOR THE PARROT BEBOP QUADCOPTER. THE MOMENTS OF INERTIA I_x, I_y, I_z ARE OBTAINED FROM [32]. ALL OTHER PARAMETERS HAVE BEEN IDENTIFIED BY MEANS OF LINEAR REGRESSION WITH SENSOR DATA OBTAINED FROM VARIOUS FLIGHTS

k_x [rpm ⁻¹ s ⁻¹]	k_y [rpm ⁻¹ s ⁻¹]	k_ω [rpm ⁻² ms ⁻²]	k_z [rpm ⁻¹ s ⁻¹]	k_h [m ⁻¹]	I_x [kgm ²]	I_y [kgm ²]	I_z [kgm ²]
1.08e-05	9.65e-06	4.36e-08	2.79e-05	6.26e-02	0.000906	0.001242	0.002054
k_p [rpm ⁻² Nm]	k_{pv} [Ns]	k_q [rpm ⁻² Nm]	k_{qv} [Ns]	k_{r1} [rpm ⁻¹ Nm]	k_{r2} [rpm ⁻¹ Nms]	k_{rr} [Nms]	τ [s]
1.41e-09	-7.97e-03	1.22e-09	1.29e-02	2.57e-06	4.11e-07	8.13e-04	0.06

with mini-batch size 256 and a starting learning rate of 1e-3.

D. Adaptive Method

We modify our model by assuming the existence of some constant external moment $\mathbf{M}_{ext} = [M_{ext,x}, M_{ext,y}, M_{ext,z}]^T$ acting on the system. The external moment can thus be considered part of our state vector $\mathbf{x} = [\mathbf{p}, \mathbf{v}, \lambda, \Omega, \omega, \mathbf{M}_{ext}]^T$. The modified system dynamics becomes:

$$\begin{aligned} \dot{\mathbf{p}} &= \mathbf{v} & \dot{\mathbf{v}} &= \mathbf{g} + R(\lambda)\mathbf{F} \\ \dot{\lambda} &= Q(\lambda)\Omega & I\dot{\Omega} &= -\Omega \times I\Omega + \mathbf{M} + \mathbf{M}_{ext} \\ \dot{\mathbf{M}}_{ext} &= 0 & \dot{\omega} &= ((\omega_{max} - \omega_{min})\mathbf{u} + \omega_{min} - \omega)/\tau \end{aligned} \quad (5)$$

Using the same approach as before, we can now generate optimal trajectories for this system and train a network to approximate the optimal state feedback. Additionally, the neural network will now have 3 extra inputs for $M_{ext,x}, M_{ext,y}, M_{ext,z}$. The obtained controller will now use these extra inputs to optimally compensate for the unmodeled moments (assuming they are constant). For the onboard implementation, we will obtain the values of \mathbf{M}_{ext} by subtracting the modeled moment (Eq. 3) from the measured moment

$$M_{measured} = I\dot{\Omega} + \Omega \times I\Omega \quad (6)$$

using filtered (8Hz 2nd order Butterworth lowpass filter) gyroscope measurements. It is important to note that the filtering causes our estimates for \mathbf{M}_{ext} to be slightly delayed. Furthermore, the controller's output is based on the assumption of a constant external moment so we can expect our method to only be effective if the modeling errors are in a sufficiently low-frequency range.

E. Differential-flatness-based Controller (DFBC)

DFBC is a state-of-the-art method for generating aggressive trajectories using piece-wise high-order polynomials $\mathbf{p}(t) = [x(t), y(t), z(t), \psi(t)]^T$ that pass through a set of waypoints while minimizing the 'Snap' defined by the following integral [4]:

$$\int_0^T \mu_r [x^{(4)}(t) + y^{(4)}(t) + z^{(4)}(t)]^2 + \mu_\psi [\psi^{(2)}(t)]^2 dt$$

In this problem, the final time is fixed, and the polynomial coefficients are found by solving a quadratic constraint optimization problem. As shown in [4], if we change the final time by a factor of α , the new minimum snap solution

is simply a time version of the original polynomial $\mathbf{p}(\alpha t)$. By changing the value of α , the trajectory can be faster or slower without having to recompute the optimal solution. In order to achieve accurate tracking, we use an outer-loop INDI controller where the velocity and acceleration feed-forward are directly computed from the polynomials.

III. EXPERIMENTAL SETUP

The quadcopter used in our experiment is the Parrot Bebop 1 which has its onboard software replaced by the Paparazzi-UAV open-source autopilot project [35]. All computations will run in real-time on the Parrot P7 dual-core CPU Cortex A9 processor. The Parrot Bebop has an MPU6050 IMU sensor that will be used to obtain measurements of the specific force and angular velocity along the body axes. Additionally, the Bebop can measure the angular velocities (in rpm) of each of the propellers, which is a requirement for our control method.

All flight tests are performed in The CyberZoo which is a research and test laboratory in the faculty of Aerospace Engineering at the TU Delft. This lab consists of a 10 by 10 meter area surrounded by nets with an OptiTrack motion capture system that can provide position and attitude data in real-time. An extended Kalman filter is used to fuse the OptiTrack and IMU data to obtain an estimate of the position, velocity, attitude and body rates. These state variables are used as input to the G&CNet along with the rpm measurements. The outputs of the network will be directly used as rpm commands to the propellers. The DFBC method will use the same state estimates to obtain the feedforward terms for the INDI controller.

IV. RESULTS & DISCUSSION

A. Nominal G&CNet

1) *Dataset and network*: Using the system dynamics from equation 1 we generate a dataset of 100,000 energy-optimal trajectories with a target state defined by $\mathbf{x}, \mathbf{v}, \lambda, \Omega, \dot{\mathbf{v}}, \dot{\Omega}, \dot{\omega} = 0$. The rpm limits are set to $\omega_{min} = 5000$, $\omega_{max} = 10000$ and the initial conditions are uniformly sampled from the following intervals:

$$\begin{aligned} x &\in [-5, 5] & y &\in [-5, 5] & z &\in [-1, 1] \\ v_x &\in [-0.5, 0.5] & v_y &\in [-0.5, 0.5] & v_z &\in [-0.5, 0.5] \\ \phi &\in [-40^\circ, 40^\circ] & \theta &\in [-40^\circ, 40^\circ] & \psi &\in [-180^\circ, 180^\circ] \\ p &\in [-1, 1] & q &\in [-1, 1] & r &\in [-1, 1] \\ \omega &\in [\omega_{min}, \omega_{max}]^4 \end{aligned}$$

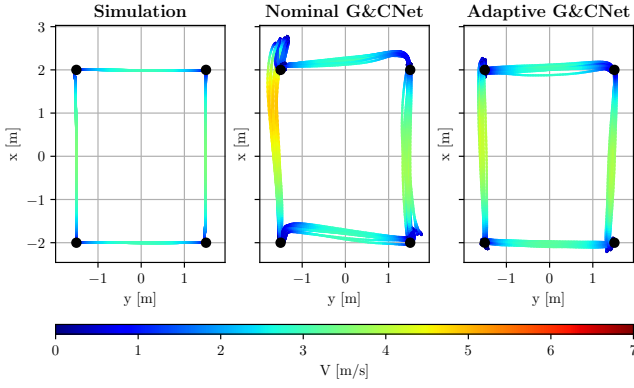


Fig. 2. Top-down view of the simulated trajectory next to the Nominal- and Adaptive G&CNet flight test

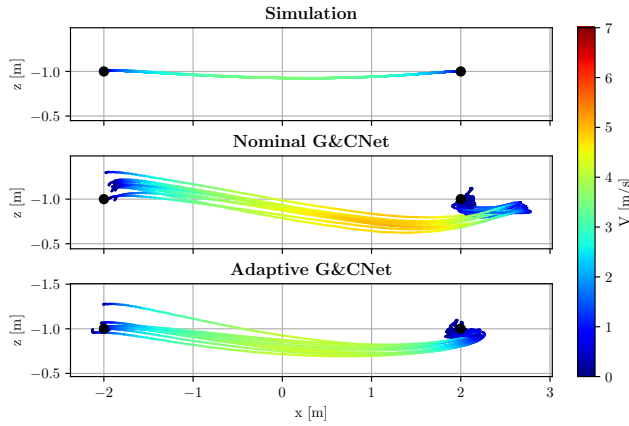


Fig. 3. Sideways view of the trajectories between waypoints 1 and 2: Simulation next to the Nominal- and Adaptive G&CNet flight test.

We split this dataset into a training set of 90,000 trajectories and a test set of 10,000 trajectories. The G&CNet is trained until a mean squared error of ~ 0.0003 is obtained on the test set.

2) *Simulation and flight test*: With the trained nominal G&CNet, we simulate the closed loop system dynamics and do a flight test where the drone flies from hover to hover in a 3×4 m rectangle. In order to fly to the target waypoints, we subtract the waypoint coordinates from the x, y and z neural network inputs. Both in simulation and the flight test, the drone flies 10 laps in which the target waypoint is switched every 4 seconds. In figure 2 a top-down view of the trajectory can be seen for the simulation and the flight test. As expected, in the simulation, the trajectories show significant overlap and the drone consistently arrives at the waypoint without overshooting. In the flight test, the trajectories are more spread out and a large deviation can be seen in the positive x -direction. The unmodeled effects are especially visible in the forward translation maneuver where the drone speeds up too much and overshoots the next waypoint. In figure 3 these forward trajectories are shown from a sideways view. It can be seen that the drone loses too much altitude causing it to speed up and overshoot.

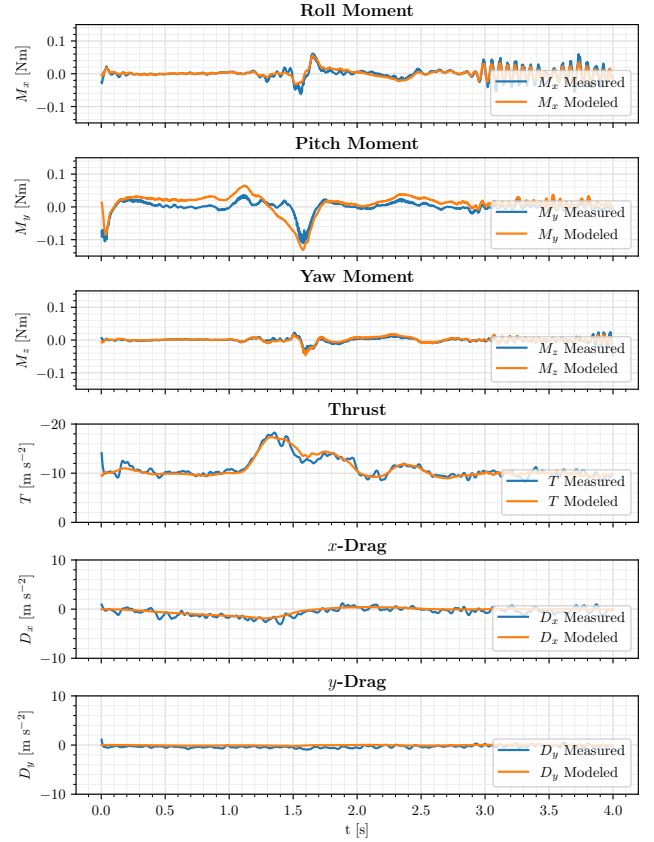


Fig. 4. Comparison of the measured and modeled moments and (specific) forces encountered in one of 'Nominal G&CNet' flights from figure 3

3) *Unmodeled Effects*: We investigate the unmodeled aerodynamic effects from the forward translation flight by comparing the measured and modeled moments and specific forces. The measured moments and forces are obtained by using the filtered (16Hz 2nd order Butterworth non-causal filter) gyroscope and accelerometer measurements. Figure 4 shows these measured and modeled quantities for one of the forward translation trajectories of the nominal G&CNet from figure 3. It can be observed that the pitch moment seems to have the most significant low-frequency model mismatch. The unmodeled pitch moment is mostly negative which might explain why the drone is diving down so much in the flight test. Because our current parametric model cannot capture this effect, we choose to go for an adaptive control strategy.

B. Adaptive G&CNet

1) *Dataset and network*: We use the modified system dynamics with external moments from equation 5 to generate another 100,000 energy-optimal trajectories with the same target state and initial conditions as before, only now we also uniformly sample the external moments from the following intervals:

$$M_{x,ext}, M_{y,ext} \in [-0.04, 0.04] \quad M_{z,ext} \in [-0.01, 0.01]$$

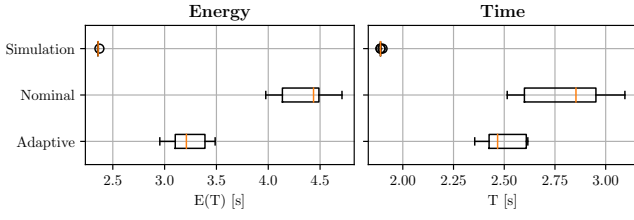


Fig. 5. Energy and time comparison during the 4m forward flight between waypoint 1 and 2: Simulation compared to Nominal and Adaptive G&CNet.

With the generated dataset we train the adaptive G&CNet with 3 extra M_{ext} inputs to learn the optimal state feedback for the modified system. Again, we train until a mean squared error of ~ 0.0003 is achieved.

2) *Performance comparison:* With the adaptive G&CNet, we perform the same flight test using the 4 waypoints and compare the results to the nominal network. In figure 2 and 3 the trajectory is compared to the previous nominal network and the simulation. It can be seen that the trajectory no longer deviates towards the positive x-direction and the overshoot in the forward translation maneuver is significantly reduced. Furthermore the box-plot in figure 5 shows the arrival time T and energy $E(T) = \int_0^T \|\mathbf{u}(t)\|^2 dt$ corresponding to the trajectories from figure 3. As one might expect, the performance gain of the adaptive network is most significant in terms of Energy. However, the arrival time and energy in the flight tests are still significantly higher than in simulation which is probably due to the overshoot at the 2nd waypoint

C. Bench-marking: Adaptive G&CNet vs. DFBC

1) *Adaptive G&CNet:* For the task of flying through consecutive waypoints, we will train an adaptive G&CNet to reach the waypoint with a forward final velocity in the direction of a 45° yaw angle. Using the modified system dynamics from Eq. 5 we generate a dataset of 10,000 energy-optimal trajectories with a target state given by:

$$x, y, z, v_z, p, q, r, \dot{p}, \dot{q}, \dot{r} = 0, v_y/v_x = \tan(\pi/4), \psi = \pi/4$$

The rpm limits are set to $\omega_{min} = 3000$, $\omega_{max} = 12000$ and the initial conditions are uniformly sampled from the following intervals:

$$\begin{aligned} x &\in [-5, -2] & y &\in [-1, 1] & z &\in [-0.5, 0.5] \\ v_x &\in [-0.5, 5] & v_y &\in [-3, 3] & v_z &\in [-1, 1] \\ \phi &\in [-40^\circ, 40^\circ] & \theta &\in [-40^\circ, 40^\circ] & \psi &\in [-60^\circ, 60^\circ] \\ p &\in [-1, 1] & q &\in [-1, 1] & r &\in [-1, 1] \\ \omega &\in [\omega_{min}, \omega_{max}]^4 \end{aligned}$$

We split this dataset into a training set of 9000 trajectories and a test set of 1000 trajectories and train until a mean squared error of ~ 0.0003 is obtained on the test set. With the trained adaptive G&CNet we perform a flight test where we fly through 4 waypoints in a 3×4 m rectangle. The controller switches to the next target waypoint and changes the coordinate system once the drone is within 1.2m from the current target. When switching to a next waypoint, we

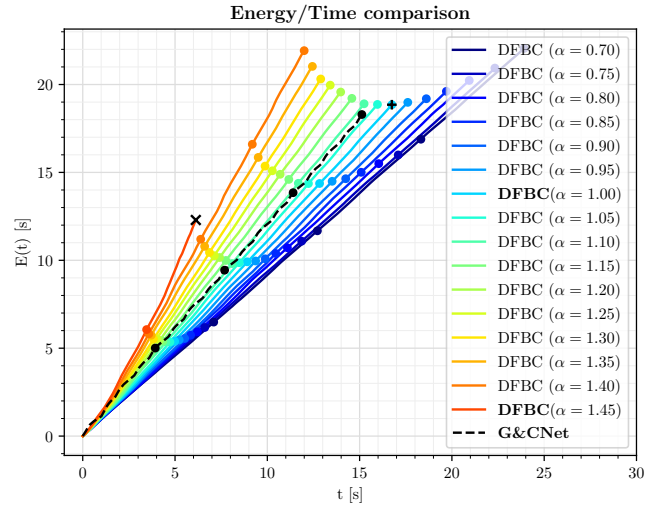


Fig. 6. Energy plotted over time during 4 laps of the 3×4 m track. The points in time where a lap is completed are represented by a dot. The DFBC method that uses the least energy is marked with a "+". The flight that crashes is marked with an "x".

rotate our coordinate system by 90° (around the z-axis) and set the next waypoint as the origin.

2) *DFBC:* We generate a piece-wise 6th order polynomial $\mathbf{p}(t) = [x(t), y(t), z(t), \psi(t)]^T$ that passes through 10 laps of the 4×3 m track with a final time of 40 seconds. To make sure the trajectory starts in hover, the initial velocity, acceleration and yaw of the trajectory are set to 0. At the 2nd waypoint, we constrain the yaw angle to be 45° which we increment by 90° for each of the following waypoints. Additionally, at these waypoints, we constrain the velocity to be aligned with the yaw direction. Using the time scaling values starting at $\alpha = 0.7$ we generate faster and faster trajectories by incrementing α by 0.05. We then track these trajectories with the INDI controller for 4 laps. We increased alpha until the INDI controller could no longer track the trajectory (which resulted in a crash at $\alpha = 1.45$).

3) *Energy/Time comparison:* We now compare the lap times and the energy integral obtained from all the flight tests. In figure 6 the energy integral $E(t) = \int_0^t \|\mathbf{u}(\tau)\|^2 d\tau$ is plotted over time for the adaptive G&CNet flight and all DFBC flights. It can be noted that the fastest DFBC method finishes the 4 laps significantly faster than the G&CNet. In terms of energy however, the adaptive G&CNet outperforms all of the DFBC methods. The DFBC method that uses the least energy ($\alpha = 1.0$) still uses more energy and time to finish the track. In figure 7, a top-down view of the trajectory of the 'energy optimal' DFBC method is plotted next to the adaptive G&CNet's flight. It can be seen that the DFBC method travels in a smooth circular trajectory at a relatively high velocity, while the G&CNet takes tighter corners and flies at a lower velocity while still finishing the 4 laps quicker.

4) *Robustness experiment:* In order to compare robustness, we apply an external moment to the drone by adding a bumper with a weight on the left side of the Bebop (Fig. 8). With this alteration, we perform the same flight tests as

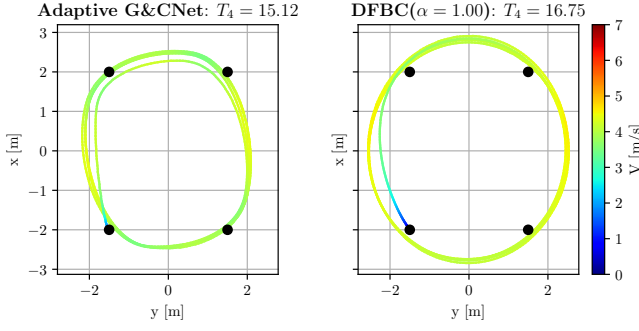


Fig. 7. Top-down view of the adaptive G&CNet's flight next to the 'energy optimal' DFBC's flight at $\alpha = 1.0$.



Fig. 8. The Parrot Bebop drone and its bumper with a weight added to it. This imbalanced weight causes a roll moment of -0.06Nm

before. In figure 9 we again show the energy/time plot for all of the performed flights. It can be seen that the time scales for the successful flight experiments using the DFBC method were limited up to $\alpha = 1.0$. In terms of time, the adaptive G&CNet demonstrated superior performance, with the quadcopter flying faster than all of the DFBC flights. The trajectories of the G&CNet and the fastest DFBC flight can be seen in figure 10. Another interesting observation is that the G&CNet flies slower with this added weight than it did in the previous flight. Here our method exhibits a clear advantage over DFBC, as it doesn't require a reference trajectory, and can dynamically adjust its course in real time. Furthermore, if we compare the rpm commands of both methods (Fig. 11) it can be seen that the G&CNet can handle sustained rpm saturations, while the DFBC method at $\alpha = 1.05$ crashes due to saturations at the same propeller.

V. CONCLUSION

We have presented a novel G&CNet setup to perform energy-optimal end-to-end control for a 3-dimensional quadcopter model (Eq. 1). With a flight test, we have investigated the real-life performance of this G&CNet which showed that unmodeled moments significantly influence flight performance. To mitigate these effects, we proposed and implemented an adaptive control strategy that shows a significant improvement in flight performance. Furthermore, we compare our proposed adaptive G&CNet to a DFBC method in consecutive waypoint flight scenarios, revealing clear advantages of our method over DFBC. Specifically, our method is more energy efficient, robust against large disturbances, and more flexible, with the ability to dynamically adjust its path in real time without relying on a reference

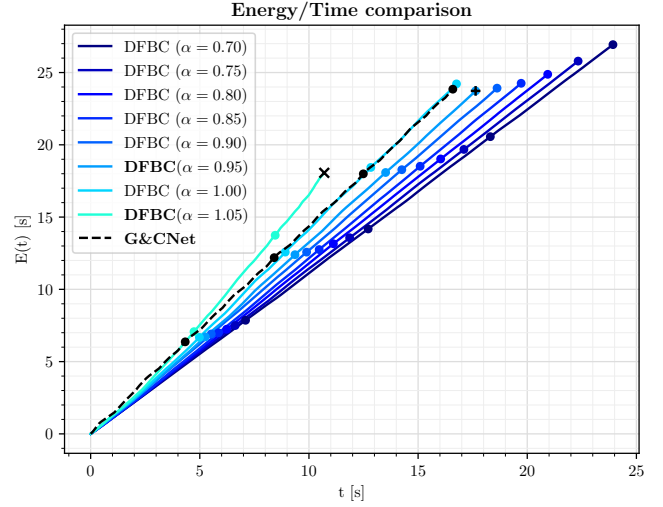


Fig. 9. Energy plotted over time during 4 laps of the $3 \times 4\text{m}$ track with the added weight. The points in time where a lap is completed are represented by a dot. The DFBC method that uses the least energy is marked with a "+". The flight that crashes is marked with an "x".

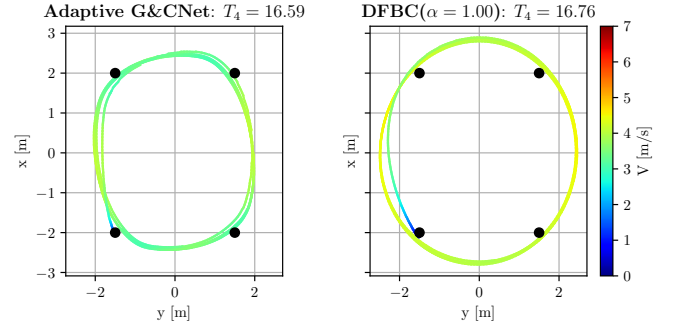


Fig. 10. Top-down view of the adaptive G&CNet's flight next to the fastest DFBC's flight at $\alpha = 1.0$ with the added weight.

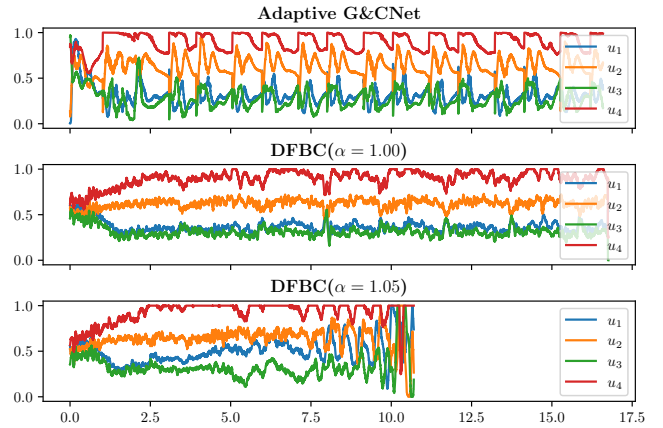


Fig. 11. Comparison of the normalized RPM commands of the Adaptive G&CNet compared to the fastest DFBC flight at $\alpha = 1.00$ and the failed flight at $\alpha = 1.05$.

trajectory.

Future work can focus on making current G&CNets time-optimal while retaining their current robustness. This could be achieved by not only compensating for the unmodeled moments but also errors in thrust, drag forces and actuator delay. Additionally, robustness could be increased by using less strict final state constraints in the optimal control problem. Finally, to improve the maneuverability of the quadcopter in turns, the G&CNet can be trained on trajectories that account for two consecutive waypoints.

ACKNOWLEDGMENT

This research was co-funded under the Discovery programme of, and funded by, the European Space Agency

REFERENCES

- [1] M. Hassanalian and A. Abdelkefi, "Classifications, applications, and design challenges of drones: A review," *Progress in Aerospace Sciences*, vol. 91, pp. 99–131, 2017.
- [2] L. Bauersfeld and D. Scaramuzza, "Range, endurance, and optimal speed estimates for multicopters," *CoRR*, vol. abs/2109.04741, 2021. [Online]. Available: <https://arxiv.org/abs/2109.04741>
- [3] M. J. Van Nieuwstadt and R. M. Murray, "Real-time trajectory generation for differentially flat systems," *International Journal of Robust and Nonlinear Control: IFAC-Affiliated Journal*, vol. 8, no. 11, pp. 995–1020, 1998.
- [4] D. Mellinger and V. Kumar, "Minimum snap trajectory generation and control for quadrotors," in *2011 IEEE International Conference on Robotics and Automation*, 2011, pp. 2520–2525.
- [5] M. Faessler, A. Franchi, and D. Scaramuzza, "Differential flatness of quadrotor dynamics subject to rotor drag for accurate tracking of high-speed trajectories," *IEEE Robotics and Automation Letters*, vol. 3, no. 2, pp. 620–626, 2017.
- [6] E. Tal and S. Karaman, "Accurate tracking of aggressive quadrotor trajectories using incremental nonlinear dynamic inversion and differential flatness," *IEEE Transactions on Control Systems Technology*, vol. 29, no. 3, pp. 1203–1218, 2020.
- [7] P. Ru and K. Subbarao, "Nonlinear model predictive control for unmanned aerial vehicles," *Aerospace*, vol. 4, no. 2, 2017. [Online]. Available: <https://www.mdpi.com/2226-4310/4/2/31>
- [8] D. Bicego, J. Mazzetto, R. Carli, M. Farina, and A. Franchi, "Nonlinear model predictive control with enhanced actuator model for multi-rotor aerial vehicles with generic designs," *Journal of Intelligent & Robotic Systems*, vol. 100, no. 3–4, pp. 1213–1247, Sep. 2020.
- [9] C. Liu, H. Lu, and W.-H. Chen, "An explicit mpc for quadrotor trajectory tracking," in *2015 34th Chinese Control Conference (CCC)*, 2015, pp. 4055–4060.
- [10] G. Torrente, E. Kaufmann, P. Foehn, and D. Scaramuzza, "Data-driven mpc for quadrotors," *IEEE Robotics and Automation Letters*, 2021.
- [11] A. Romero, S. Sun, P. Foehn, and D. Scaramuzza, "Model predictive contouring control for near-time-optimal quadrotor flight," *CoRR*, vol. abs/2108.13205, 2021. [Online]. Available: <https://arxiv.org/abs/2108.13205>
- [12] A. Romero, R. Penicka, and D. Scaramuzza, "Time-optimal online replanning for agile quadrotor flight," *IEEE Robotics and Automation Letters*, vol. 7, no. 3, pp. 7730–7737, Jul. 2022.
- [13] S. Sun, A. Romero, P. Foehn, E. Kaufmann, and D. Scaramuzza, "A comparative study of nonlinear mpc and differential-flatness-based control for quadrotor agile flight," *IEEE Transactions on Robotics*, 2022.
- [14] D. Hanover, P. Foehn, S. Sun, E. Kaufmann, and D. Scaramuzza, "Performance, precision, and payloads: Adaptive nonlinear mpc for quadrotors," *IEEE Robotics and Automation Letters*, vol. 7, no. 2, pp. 690–697, 2022.
- [15] P. Foehn, A. Romero, and D. Scaramuzza, "Time-optimal planning for quadrotor waypoint flight," *Science Robotics*, vol. 6, no. 56, p. eabh1221, 2021.
- [16] M. W. Mueller, M. Hehn, and R. D'Andrea, "A computationally efficient motion primitive for quadcopter trajectory generation," *IEEE Transactions on Robotics*, vol. 31, no. 6, pp. 1294–1310, 2015.
- [17] S. Tankasala, C. Pehlivanurk, E. Bakolas, and M. Pryor, "Smooth time optimal trajectory generation for drones," *arXiv preprint arXiv:2202.09392*, 2022.
- [18] M. Geisert and N. Mansard, "Trajectory generation for quadrotor based systems using numerical optimal control," *CoRR*, vol. abs/1602.01949, 2016. [Online]. Available: <http://arxiv.org/abs/1602.01949>
- [19] Y. Mao, M. Szmuk, X. Xu, and B. Açikmese, "Successive convexification: A superlinearly convergent algorithm for non-convex optimal control problems," *arXiv preprint arXiv:1804.06539*, 2018.
- [20] Y. Yu, K. Nagpal, S. Mceowen, B. Açikmeşe, and U. Topcu, "Real-time quadrotor trajectory optimization with time-triggered corridor constraints," *arXiv preprint arXiv:2208.07259*, 2022.
- [21] Y. Song, M. Steinweg, E. Kaufmann, and D. Scaramuzza, "Autonomous drone racing with deep reinforcement learning," in *2021 IEEE/RSJ International Conference on Intelligent Robots and Systems (IROS)*. IEEE, 2021, pp. 1205–1212.
- [22] G. Tang, W. Sun, and K. Hauser, "Learning trajectories for real-time optimal control of quadrotors," *IEEE/RSJ Intl Conf on Intelligent Robots and Systems*, 2018. [Online]. Available: <https://par.nsf.gov/biblio/10100589>
- [23] Q. Li, J. Qian, Z. Zhu, X. Bao, M. K. Helwa, and A. P. Schoellig, "Deep neural networks for improved, impromptu trajectory tracking of quadrotors," in *2017 IEEE International Conference on Robotics and Automation (ICRA)*. IEEE, 2017, pp. 5183–5189.
- [24] S. Li, Y. Wang, J. Tan, and Y. Zheng, "Adaptive rbfnns/integral sliding mode control for a quadrotor aircraft," *Neurocomputing*, vol. 216, pp. 126–134, 2016. [Online]. Available: <https://www.sciencedirect.com/science/article/pii/S0925232116307780>
- [25] J. Hwangbo, I. Sa, R. Siegwart, and M. Hutter, "Control of a quadrotor with reinforcement learning," *IEEE Robotics and Automation Letters*, vol. 2, no. 4, pp. 2096–2103, 2017.
- [26] E. Kaufmann, A. Loquercio, R. Ranftl, M. Müller, V. Koltun, and D. Scaramuzza, "Deep Drone Acrobatics," in *RSS: Robotics, Science, and Systems*. Corvallis, Oregon, USA: Robotics: Science and Systems Foundation, jul 2020, pp. 1–10.
- [27] S. Li, E. Öztürk, C. De Wagter, G. C. H. E. de Croon, and D. Izzo, "Aggressive online control of a quadrotor via deep network representations of optimality principles," in *2020 IEEE International Conference on Robotics and Automation, ICRA 2020*, ser. Proceedings - IEEE International Conference on Robotics and Automation. United States: Institute of Electrical and Electronics Engineers (IEEE), May 2020, pp. 6282–6287.
- [28] C. Sánchez-Sánchez and D. Izzo, "Real-time optimal control via deep neural networks: Study on landing problems," *Journal of Guidance, Control, and Dynamics*, vol. 41, 10 2016.
- [29] D. Tailor and D. Izzo, "Learning the optimal state-feedback via supervised imitation learning," *Astrodynamics*, vol. 3, no. 4, pp. 361–374, 2019.
- [30] E. J. J. Smeur, Q. Chu, and G. C. H. E. de Croon, "Adaptive incremental nonlinear dynamic inversion for attitude control of micro air vehicles," *Journal of Guidance, Control, and Dynamics*, vol. 39, no. 3, pp. 450–461, Mar. 2016.
- [31] J. Svacha, K. Mohta, and V. R. Kumar, "Improving quadrotor trajectory tracking by compensating for aerodynamic effects," *2017 International Conference on Unmanned Aircraft Systems (ICUAS)*, pp. 860–866, 2017.
- [32] S. Sun, C. C. de Visser, and Q. Chu, "Quadrotor gray-box model identification from high-speed flight data," *Journal of Aircraft*, vol. 56, no. 2, pp. 645–661, Mar. 2019.
- [33] R. Fourer, D. M. Gay, and B. W. Kernighan, "A modeling language for mathematical programming," *Management Science*, vol. 36, no. 5, pp. 519–554, 1990.
- [34] P. E. Gill, W. Murray, and M. A. Saunders, "Snopt: An sqp algorithm for large-scale constrained optimization," *SIAM review*, vol. 47, no. 1, pp. 99–131, 2005.
- [35] B. Gati, "Open source autopilot for academic research - the paparazzi system," in *2013 American Control Conference*. IEEE, Jun. 2013.